AIP Advances

RESEARCH ARTICLE | SEPTEMBER 26 2024

Employing nutraceutical industry by-product, cumin seeds spent, for the adsorption treatment of acid blue 113 dye

Syed Noeman Taqui; Usman Taqui Syed; Sameer Algburi ; Rayees Afzal Mir; Akheel Ahmed Syed ;
Abdullah I. Al-Mansour; Shamshad Alam ; Mohammad Amir khan ; Shareefraza J. Ukkund

Check for updates

AIP Advances 14, 095034 (2024)
https://doi.org/10.1063/5.0217877

View Online
Export Citation

Articles You May Be Interested In

Caulerpa lentillifera as a potential nutraceutical resource

AIP Conf. Proc. (January 2023)

In silico analysis of the potential of *Sargassum sp* brewed and *Syzygium polyanthum* leaf as nutraceuticals

AIP Conf. Proc. (January 2023)

A vascular-liver chip for sensitive detection of nutraceutical metabolites from human pluripotent stem cell derivatives

Biomicrofluidics (May 2020)

06 March 2025 15:32:30

AIP Publishing

Special Topics Open for Submissions

Learn More

AIP Publishing

Employing nutraceutical industry by-product, cumin seeds spent, for the adsorption treatment of acid blue 113 dye

Cite as: AIP Advances 14, 095034 (2024); doi: 10.1063/5.0217877
Submitted: 7 May 2024 • Accepted: 23 August 2024 •
Published Online: 26 September 2024

View Online Export Citation CrossMark

Syed Noeman Taqui,[1,a] Usman Taqui Syed,[2,b] Sameer Algburi,[3,c] Rayees Afzal Mir,[4,d] Akheel Ahmed Syed,[5,e] Abdullah I. Al-Mansour,[6,f] Shamshad Alam,[6,g] Mohammad Amir khan,[7,e] and Shareefraza J. Ukkund[8,h]

AFFILIATIONS

[1] Department of Chemistry, Bharathi College-Post Graduate and Research Centre, Bharathi Nagara, Karnataka 571422, India
[2] LAQV-REQUIMTE, Department of Chemistry, Faculty of Science and Technology, Universidade NOVA de Lisboa, 2829-516 Caparica, Portugal
[3] Al-Kitab University, Kirkuk, Iraq
[4] Glocal School of Agricultural Science, Glocal University, Mirzapur pole, Saharanpur, Uttar Pradesh 247121, India
[5] Centre for Advanced Research and Innovation, Glocal University, Delhi-Yamunotri Marg, SH - 57, Mirzapur Pole, Saharanpur District, Uttar Pradesh 247121, India
[6] Department of Civil Engineering, College of Engineering, King Saud University, Riyadh 11421, Saudi Arabia
[7] Department of Civil Engineering, Galgotias College of Engineering, Knowledge Park 11, Greater Noida 201310, India
[8] Department of Biotechnology, P. A. College of Engineering, Mangalore 574153, India

[a] noemansyed89@gmail.com
[b] s.taqui@campus.fct.unl.pt
[c] sameer.algburi@uoalkitab.edu.iq
[d] raies.afzal@gmail.com
[e] **Authors to whom correspondence should be addressed:** akheelahmed54@gmail.com and amirmdamu@gmail.com
[f] amansour@ksu.edu.sa
[g] salam@ksu.edu.sa
[h] drshareef2022@gmail.com

ABSTRACT

The aim of this study is to discover the potential use of nutraceutical industrial cumin seed spent (NICUS) as an economical biosorbent for eliminating acid blue 113 (AB113), an azo dye, from water. The study investigates the influence of pH, adsorbent dosage, temperature, particle size, and initial dye concentration on the adsorption of AB113. Various isotherm models and kinetic models were studied. At equilibrium situations, the maximum trial adsorption volume (q_e) was found to be 96 mg g^{-1}. The main objective was to determine the suitability of the pseudo-second-order model for describing the kinetics of adsorption. Thermodynamic parameters ΔG^0 ΔH^0 ΔS^0 revealed that the adsorption process was endothermic and non-spontaneous. The lower value of ΔH^0 suggests a physical adsorption process. Analysis using FTIR and SEM spectra confirmed that the NICUS surface effectively adsorbed AB113. NICUS emerges as a promising adsorbent for the efficient deduction of AB113 from aqueous solutions.

© 2024 Author(s). All article content, except where otherwise noted, is licensed under a Creative Commons Attribution-NonCommercial 4.0 International (CC BY-NC) license (https://creativecommons.org/licenses/by-nc/4.0/). https://doi.org/10.1063/5.0217877

06 March 2025 15:32:30

I. INTRODUCTION

Cumin seed production is primarily concentrated in India, which accounts for 73% of global production and 80% of its consumption. Other significant producers include Iran (4%), Turkey (3%), and Syria (7%), with the remaining 6% coming from various other countries.[1] Annually, ~400 000 metric tons of cumin seeds are produced.[2] The cost of cumin seeds varies based on factors such as quantity, quality, variety, location, season, and demand, typically ranging from $2.2 to $4 per kilogram.[3]

Cumin, the dehydrated seed of the Cuminum cyminum L plant, belongs to the parsley family. The plant features a key stem branching into up to five subordinate divisions, both with 2–3 sections, resulting in a uniform canopy. The stems are branched, glabrous, 3–5 cm in diameter, typically dull green in color, with alternate leaves that are lanceolate, slightly hairy, and bluish-green petioles.[4]

The inflorescence of cumin consists of complex umbels of white or pinkish flowers with thread-like leaflets that are pinnate or bipinnate. The small flowers are arranged in umbels with 5–7 umbellates per umbel. The fruit, a schizocarp, is 4–5 mm long and has two mericarps enclosing a single seed. These fruits are oval or fusiform lateral achenes with eight ridges containing oil tubes.[5] The seeds, similar in arrival to fennel and anise seeds but minor and gloomier, may have noticeable hairs depending on the variety.

The aim of the current study is to subsidize environmental sustainability by utilizing nutraceutical industrial cumin seed waste (NICUS) for bioremediation. Specifically, the study focuses on removing acid blue 113 (AB113) from the effluent of the textile industry. Recent efforts at our research institute have explored creating composites using Nutraceutical Industrial Spent (NIS) as a filler material[6] and as a bioadsorbent for removing harmful dyes.[7,8] Pilot-scale demonstrations have highlighted the potential of NIS in circular economics.[9]

The primary aim was to evaluate whether the cost-effective biosorbent NICUS could effectively remove AB113 from aqueous solutions. This approach highlights the use of nutraceutical industrial spent as an environmentally friendly and affordable solution to mitigate dye toxicity in textile industry wastewater. The study includes modeling studies and a scrutiny of the economics of biosorbent regeneration to support experimental findings.

FIG. 1. Images of the process used to obtain the cumin seed spent powder from unprocessed commercially available cumin seeds.

II. MATERIALS, PREPARATION, AND CHARACTERIZATION

A. Materials

The Acid Blue 113 (AB113) dye was procured from Sigma-Aldrich in the USA.

B. Characterization and preparation of adsorbent

1. Adsorbent

NICUS was sourced from a local factory specializing in oleoresin extraction from cumin seeds (Fig. 1). The NICUS underwent a process involving air drying, pulverization, crushing using a ball mill, and sieving rendering to American Society for Testing and Materials (ASTM) standards.

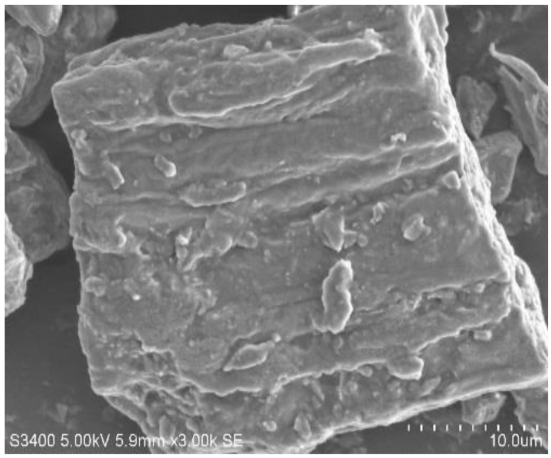

FIG. 2. SEM image of NICUS.

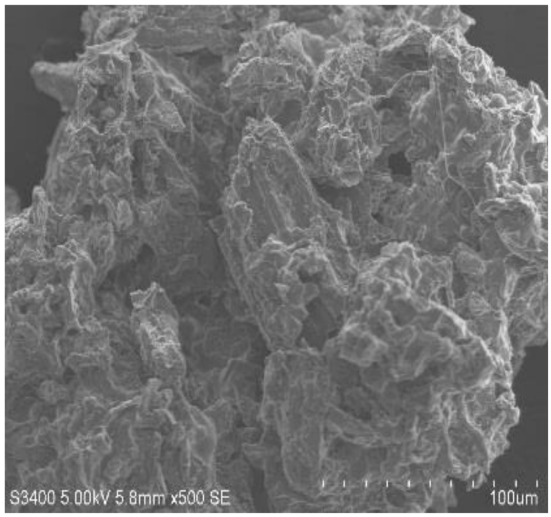

FIG. 3. SEM image of AB113-NICUS.

06 March 2025 15:32:30

© Author(s) 2024

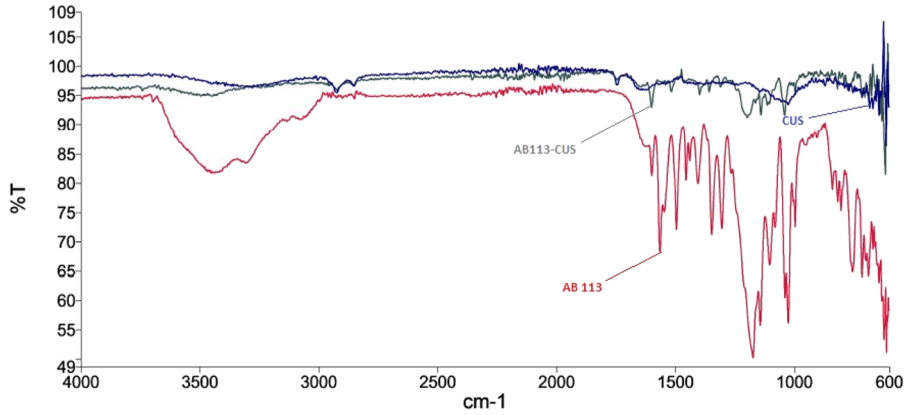

FIG. 4. FTIR spectra of NICUS, AB113 dye, and AB113 dye adsorbed onto NICUS.

2. Surface characterization

The surface morphology of NICUS was analyzed with a scanning electron microscope (LEO 435 VP model, Japan). The functional groups present in the adsorbent were identified using Fourier Transform Infrared Spectroscopy (FTIR). Infrared spectra were recorded for both control samples (NICUS without AB113 adsorption) and samples loaded with AB113 using an FTIR spectrometer (Inter-spec 2020, Spectrolab, UK). The point of zero charge (pHz) was established as a reference for NICUS.

III. RESULTS AND DISCUSSION

A. Adsorbent's surface Characterization

Due to the occurrence of cellulose and lignocellulose facilities, NICUS exhibits an obviously amorphous and fibrous morphology.[10] Scanning Electron Microscopy (SEM) investigation of the NICUS surface exposed a complex porous structure (Fig. 2). Upon adsorption of the adsorbate (AB113 dye), some of these pores become completely filled, forming a distinct layer on the surface (Fig. 3). The functional groups present in NICUS were identified through IR spectroscopy analysis (Fig. 4). The wideband observed in the IR spectrum of NICUS between 3100 and 3500 cm^{-1} is due to the hydroxyl groups in cellulose and adsorbed water molecules. Additionally, bands at 1600 cm^{-1} (C–H stretching) and a weak, sharp band at 3000 cm^{-1} (C–O stretching) were also detected. Furthermore, bands at 1330, 1300, 1240, 1210, and 1010 cm^{-1} indicate C–O–C stretching. After the adsorption of AB113 dye onto NICUS, changes in the IR spectra were noted. The broadbands between 3200 and 3550 cm^{-1}, attributed to N–H widening in the $–NH_2$ group of AB113 dye, disappeared, indicating hydrogen bonding formation between $–NH_2$ groups of the dye and hydroxyl groups of NICUS. Similarly, the withdrawal of a prominent peak at 1500 cm^{-1}, corresponding to N–N stretching in AB113 dye, further approves resilient adsorption of the dye onto NICUS. Based on the shift in IR absorption frequencies, it can be concluded that AB113 dye has effectively adsorbed onto NICUS. The point of zero charge (pHz) of NICUS was determined to be pH 7.40 (Fig. 5), indicating the pH at which the surface charge of NICUS is neutral.

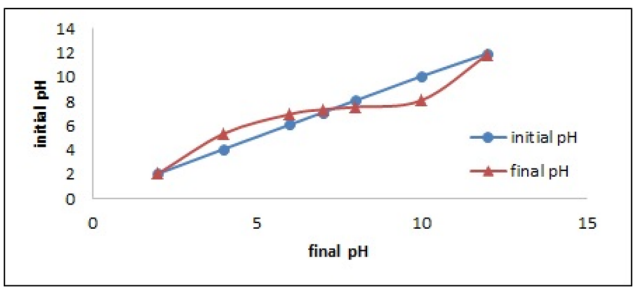

FIG. 5. The point of zero charge for NICUS.

B. Impact of initial dye concentration and pH

To achieve maximum adsorption capacity, optimal conditions must be determined. pH significantly influences the surface properties of the adsorbent and the ionization state of the dye molecules in solution, thereby controlling the adsorption process.[11] In this study, the highest adsorption volume was observed at pH 2 (Fig. 6).

C. Adsorbent dosage effect

The number of adsorbent units used directly influences the adsorption process by determining how much adsorbate can be removed under specific operating conditions. In this study, the capacity of NICUS to absorb AB113 dye was investigated across varying amounts of adsorbent (0.02–0.300 g in 50 ml of solution). It was witnessed that increasing the amount of adsorbent resulted in greater removal of AB113 dye.[12] As more NICUS was added, additional AB113 dye molecules were absorbed onto the surface of the adsorbent, beyond what was shown in Fig. 6, where maximum adsorption capacity was observed at pH 2. Eventually, a point of saturation was reached where dye molecules began to bind to the outer layer of the adsorbent once the equilibrium between dye molecules in solution and adsorbed on the adsorbent was achieved. Figure 6 illustrates these findings.

06 March 2025 15:32:30

© Author(s) 2024

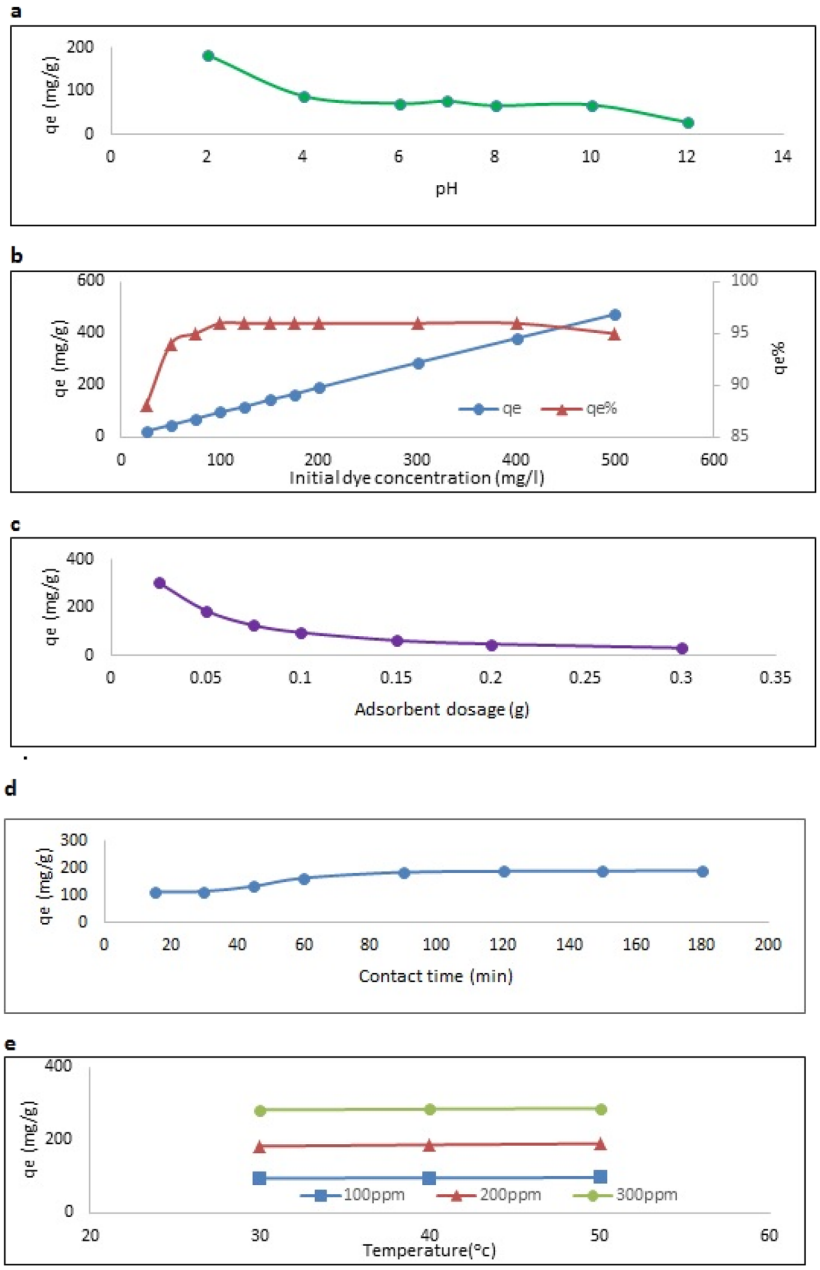

FIG. 6. Experimental variables contain (a) pH, (b) initial dye concentration in relation to the percentage of q_e, (c) dosage adsorbent, (d) time of contact, and (e) temperature.

D. Impact of contact time on dye uptake

The adsorption of AB113 dye onto NICUS was conducted for different durations—15, 30, 45, 60, 90, 120, 150, and 180 min—to evaluate the effect of contact time. It was observed that rapid adsorption occurred initially, reaching ~80% within the first 60 min. Subsequently, adsorption continued at a slower rate, reaching equilibrium after about 180 min. These results are depicted in Fig. 6. Dyes molecules gather deeper and more widely inside the adsorbent's structure as the contact time rises. However, the effectiveness of prolonged contact time diminishes as mesopores become filled, hindering further diffusion of dye molecules into the adsorbent.

06 March 2025 15:32:30

© Author(s) 2024

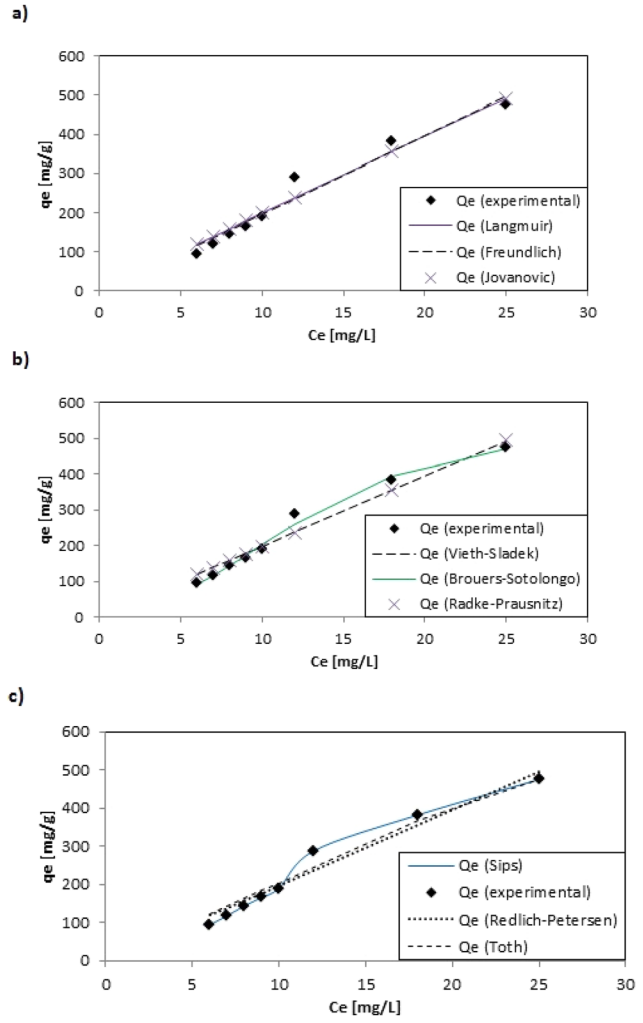

FIG. 7. Suitable adsorption to (a) Jovanovic, Langmuir, Freundlich models, (b) Brouers–Sotolongo, Vieth–Sladek, Radke–Prausnitz models, and (c) Redlich–Petersen, Sips, and Toth adsorption isotherm models.

E. Effect of temperature

The adsorption experiments were conducted over a temperature range of 30–50 °C using three different initial dye concentrations, as illustrated in Fig. 6. It is evident from the results that as the temperature increases, the adsorption volume gradually decreases, representing an endothermic nature of the adsorption process. The dye molecules are more mobile at higher temperatures, characterized by lower activation energy and faster intra-molecular diffusion rates, and may contribute to increased adsorption capacities observed at advanced temperatures.[13]

F. Adsorption isotherm

Adsorption isotherm models can be used to describe the adsorption of adsorbate particles onto adsorbent exteriors, each capturing different aspects of the process: Langmuir isotherm model,[14] the dimensionless separation factor R_L,[15] Freundlich isotherm model,[16] and Jovanovic isotherm model.[17] It provides a more flexible approach compared to the classical Langmuir isotherm model. The homogeneity or heterogeneity of the system was not entirely explained by the Langmuir and Freundlich models when it came to the experimental setting of AB113 dye adsorption on NICUS. Therefore, more complex models such as the Jovanovic isotherm (Fig. 7) were explored to better fit the experimental data and understand the adsorption behavior more comprehensively. Table I shows the strategic boundaries of two-structure isotherms.

TABLE I. Strategic boundaries of two-structure isotherms.

Langmuir		Freundlich		Jovanovic	
Q_m	29 554.14	K_F	18.83	Q_m	14 322.75
K_S	0.001	n_F	0.983	K_J	0.001

The Redlich–Peterson isotherm model,[18] Brouers–Sotolongo isotherm model,[19] and Vieth–Sladek isotherm model[20] are related and are depicted in Fig. 7 and Table II. The Sips isotherm model,[21] Toth isotherm model,[22] and Radke–Prausnitz isotherm model[23] projected a Q_m value of 1.80 mg g^{-1}, which differed significantly from the experimentally achieved q_e value, indicating limitations in its applicability to this specific adsorption system. Finally, it is important to note that higher-order models are utilized to better describe complex adsorption mechanisms. The determination coefficient R^2 applies only to linear models and should not be used to validate data fitting for nonlinear models. Table III summarizes the criteria for the three critical parameters (Q_m, χ^2, and R^2). Discrepancies between model-predicted values and experimental data (q_e) are of interest to researchers, particularly in developing new models that can provide a more accurate understanding of adsorption behaviors in systems involving NIS (Nutraceutical Industrial Spent) and dyes.

G. Kinetics of adsorption

Possible phases of the adsorption series that control rate were identified through the analysis of kinetic models. AB113 dye concentrations of 100, 200, and 300 ppm were used in the kinetic investigations. The differences in adsorption rates at 303, 313, and 323 K are demonstrated by kinetic tests. Several kinetic models were applied to the adsorption kinetics data for non-linear analysis, including the pseudo-first order,[24] pseudo-second order,[25] Weber–Morris intra-particle diffusion model,[26] Dumwald–Wagner model,[27] and film diffusion model[28] (MS Excel 2010). The computed limits are shown in Table IV.

Factors of persistence (R^2) and chi-square values (χ^2) show that at all preliminary AB113 dye concentrations (100, 200, and 300 ppm) at varied temperatures, the pseudo-second order model suited the experimental data in Fig. 8 restored than the pseudo-first order model. After reaching its peak, the degree of adsorption progressively dropped until it came to a stop. As the temperature rose, the adsorption limit grew (q_e). These results validate that there is no rate limitation in the adsorption operations. Additionally, the results suggest that the solute particles moved from the mass response for the strong surface to the NICUS pores during the initial stages of the adsorption interaction.

06 March 2025 15:32:30

© Author(s) 2024

TABLE II. Strategic boundaries of three-structure isotherms.

Redlich–Peterson		Toth		Sips		Vieth–Sladek		Brouers–Sotolongo		Radke–Prausnitz	
A_{RP}	20.4	Q_m	480.1	Q_m	844.1	Q_m	29 535.5	Q_m	498.3	Q_m	1.8
B_{RP}	0.031	n_{T0}	22.124	K_s	1.879	K_{VS}	0.017	K_{BS}	0.007	k_{rp}	11.113
g	0	b_{T0}	2.27E+30	m_s	27.066	β_{VS}	0.001	A	1.868	m_{rp}	0

TABLE III. Arithmetical limitations for suitable isotherm model.

Isotherms	Langmuir	Freundlich	Jovanovic	Radke–Prausnitz	Redlich–Peterson	Toth	Sips	Vieth–Sladek	Brouers–Sotolongo
SSE	5041.5	5018.6	5041.1	5054.4	5054.4	4382.4	1307.5	5041.5	1231.6
χ^2	24.939	22.322	24.974	24.082	24.082	26.208	6.156	24.939	4.681
R^2	0.96	0.96	0.96	0.96	0.96	0.98	0.99	0.96	0.99

TABLE IV. Constraints for theoretically predicted and experimentally determined representations.

			Pseudo-first order				Pseudo-second order			
Initial concentration [ppm]	Temp (K)	$q_{e\ Expt.}$ $(mg\,g^{-1})$	$Q_{m\ pred}$ $(mg\,g^{-1})$	k_1	R^2	χ^2	$Q_{m\ pred}$ $(mg\,g^{-1})$	k_2	R^2	χ^2
	303	96	89.08	1.54×10^{-1}	0.77	4.40	105.62	1.81×10^{-3}	0.85	10.20
100	313	97	92.05	3.67×10^{-1}	0.60	1.13	98.26	7.79×10^{-3}	0.79	0.57
	323	98	93.28	3.58×10^{-1}	0.99	0.03	99.05	8.02×10^{-3}	0.96	0.08
	303	184	200.71	9.43×10^{-2}	0.76	19.03	256.36	3.70×10^{-4}	0.78	15.93
200	313	188	189.37	1.89×10^{2}	0.97	1.29	65.88	1.71×10^{-3}	0.76	1.65
	323	191	124.16	2.94×10^{-1}	0.47	0.30	127.60	8.41×10^{-3}	0.79	0.12
	303	284	244.86	9.92×10^{-2}	0.57	36.85	299.75	3.79×10^{-4}	0.61	28.16
300	313	286	269.13	2.30×10^{-1}	0.66	9.46	303.82	1.12×10^{-3}	0.82	4.87
	323	288	285.74	1.55×10^{-1}	0.96	2.62	347.35	4.96×10^{-4}	0.93	4.77

The Dumwald–Wagner model [Fig. 9(a)] calculates the true absorption rate constant (K), accounting for practical dispersion parameters (Table V). In the Weber–Morris model [Fig. 9(b)], over the course of the interaction, the solute approval fluctuates with $t^1/_2$. Adsorption energy is often managed by a variety of factors. Our investigational results demonstrate that there are multiple linearity levels at every solute focus. The adsorption rate is strong at lower temperatures and lower initial fixations (100 ppm). The pace eventually equalizes in terms of time after proceeding in a different direct direction. Nevertheless, the amount is more direct at higher temperatures. At higher solute fixations (300 ppm), there is less noticeable variation in the adsorption rate. This is especially clear when the Boyd *et al.* film dispersion model is used to fit data at higher temperatures. Figure 9(c) shows excellent values for R^2 and χ^2, indicating that the data fit the model well, and it gives the liquid film diffusion constant $R|$ (Table V). This demonstrates that at advanced temperatures, diffusional constraints only slightly slowed the rate of adsorption. Distribution is a rate-restricting interaction, as one might expect. The reason why the retention rates change over time is because after it is rapidly ingested, the solute coats the outer layer of the particles.

H. Adsorption thermodynamics

An important role for energy and entropy is assumed in the connection cycle design. Figures 10 and 11 illustrate how to calculate $\Delta H°$ and $\Delta S°$.

Table VI presents the evaluations for the thermodynamic parameters. A positive result for $\Delta S°$ demonstrates the acute taste of the AB113 color for the adsorbent as well as the extended randomization at the surface of the strong arrangement. The unusually low upsides of $\Delta H°$ imply that the adsorption component is physical, since enthalpy changes of >200 kJ mol^{-1} are frequently observed during material activities. Table VI shows that, using the dynamic parameters from the pseudo-second-order model and the Arrhenius equation, the activation energy values for the adsorption process increased from ~100.29 to 1055.99 $kJmol^{-1}$ at different initial concentrations (100, 200, and 300 ppm).

I. Real progress via a disjointed factorial test scheme

Discovering and adapting a reasonable model regression to the experimental data obtained through the use of a fractional facto-

06 March 2025 15:32:30

© Author(s) 2024

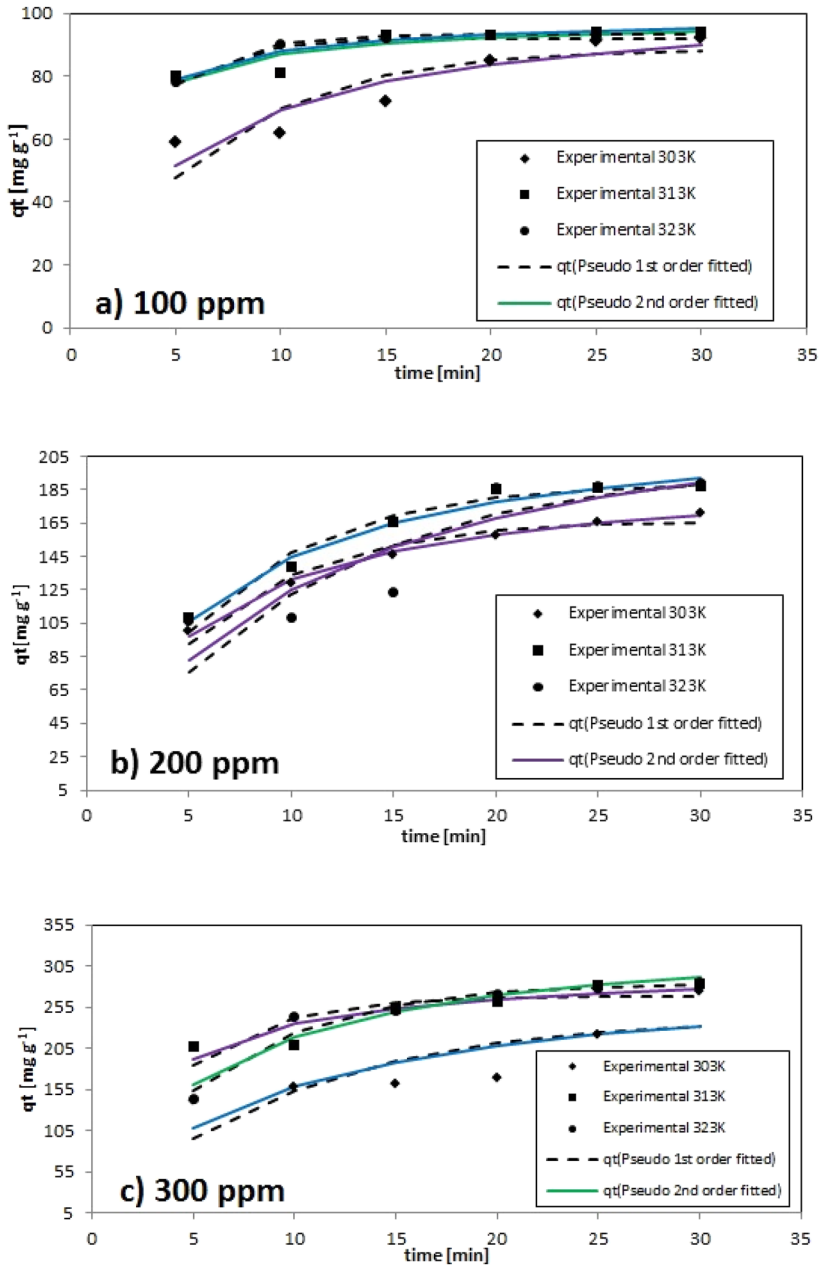

FIG. 8. Kinetic model fitting of AB113 dye on the NICUS system of (a) 100, (b) 200, and (c) 300 ppm at various temperatures.

rial experimental design (FFED) was the most crucial step in the streamlining process.

The quadratic decline revision of variance (Table VII) kind's manifest just how vital all of these elements are both as distinct and group properties. The actual against predicted value analysis figure (Fig. 12) demonstrates a strong link between the experiment and expected responses. The relapse condition of the review is displayed below:

$$\begin{aligned}\textbf{Adsorption} = {} & -10.5 + 69.2 * A + 15.6 * B + 197.3 * C \\ & -99.8 * D - 71.8 * E + 12.0 * AB + 70.9 * AC \\ & +32.2 * BC - 67.5 * A^2 - 14.8 * B^2 + 0.1 * C^2 \\ & +104.5 * D^2 + 53.0 * E^2\end{aligned}$$

The optimal conditions for the statistical optimization experiment included a pH of 2.2, an adsorbent concentration of 6.000 gL^{-1},

06 March 2025 15:32:30

© Author(s) 2024

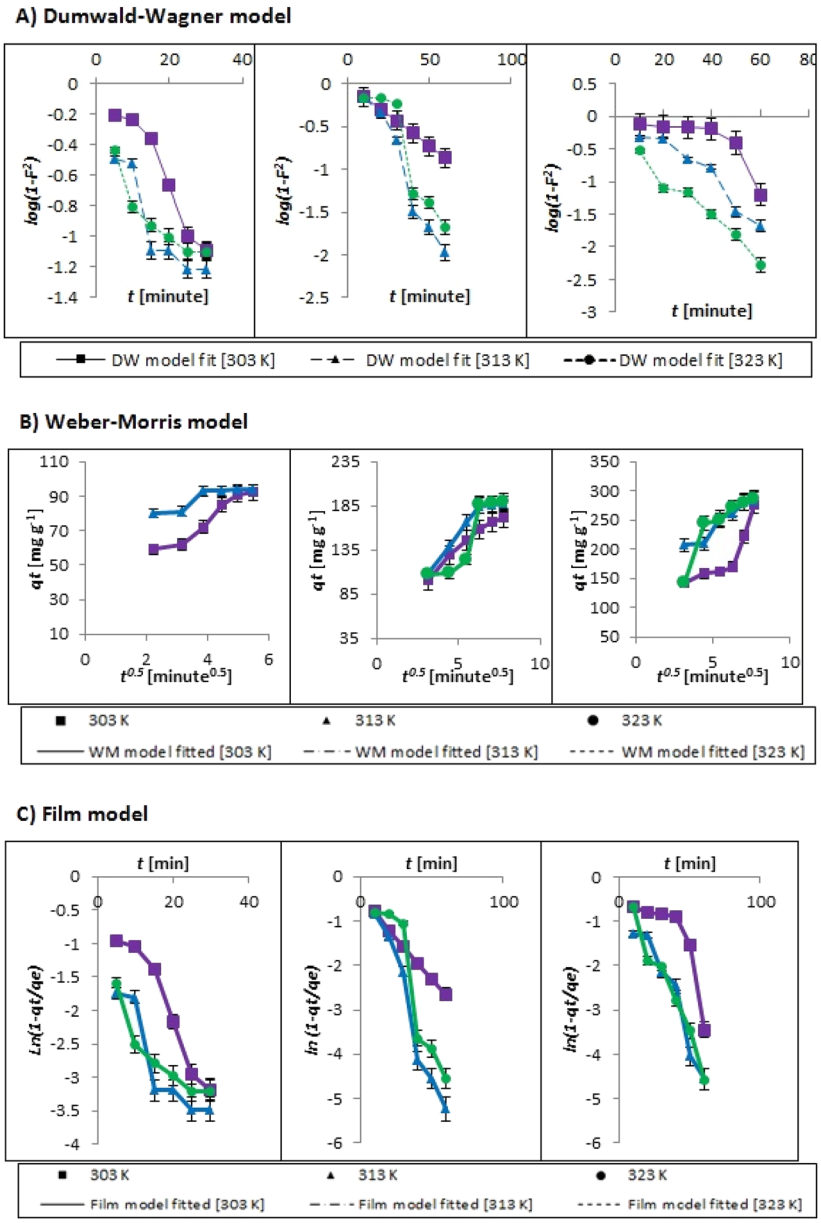

FIG. 9. Kinetic models: (A) Dumwald–Wagner model, (B) Weber–Morris model, and (C) the film model were applied to fit the adsorption of AB113 dye onto the NICUS system at concentrations of 100, 200, and 300 ppm, across different temperatures.

and an initial dye concentration of 693.00 mgL^{-1}. The adsorption process was carried out for 132.00 min with orbital shaking at 165 rpm and a temperature of 55 °C. The supreme adsorption consequence was 810.50 mg g^{-1}.

Statistical process optimization allows one to evaluate the effect of the process parameters on adsorption as well as calculate the ideal condition within a predefined range of parameter values. Adsorption capacity improves with time, as shown by 3D graphs that link time with other variables. By optimizing temperature, duration, particle size, and dye concentration, we can accelerate the adsorption process. The maximum adsorption was achieved at 132 minutes. Adsorption capacity benefits from an increase in temperature. Temperature increases and the passage of time both increase adsorption capability. The optimal pH for increased adsorption capacity is about 2.2; above this, increasing the pH has a negative effect on the sorption size. Positive values signify an increasing effect; for example, an increase in temperature (B) causes a substantial increase in sorption capacity. As a result, the surface and contour plots offer a

06 March 2025 15:32:30

© Author(s) 2024

TABLE V. Strategic boundaries for diffusion illustrations.

Initial concentration (ppm)	Temp (K)	Film diffusion model		Weber–Morris model		Dumwald–Wagner	
		$R^{\|}$ (min^{-1})	R^2	k_{ist} [mg g^{-1} $s^{-0.5}$]	R^2	K (min^{-1})	R^2
100	303	0.1009	0.94	11.75	0.94	0.092	0.94
	313	0.0783	0.80	5.02	0.80	0.075	0.81
	323	0.0589	0.82	4.46	0.76	0.056	0.83
200	303	0.0373	0.99	15.48	0.97	0.033	0.99
	313	0.0957	0.96	18.18	0.92	0.091	0.95
	323	0.0868	0.87	22.10	0.83	0.081	0.87
300	303	0.0458	0.65	25.94	0.75	0.041	0.62
	313	0.0710	0.92	19.08	0.92	0.068	0.92
	323	0.0711	0.97	27.89	0.81	0.074	0.97

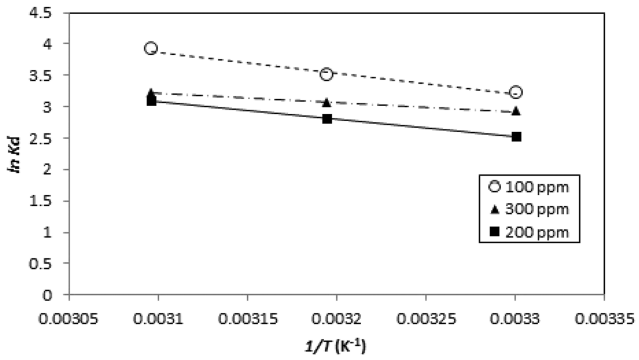

FIG. 10. The enthalpy and Gibbs free energy of the process were determined by graphing the thermodynamic constants as a function of 1/T.

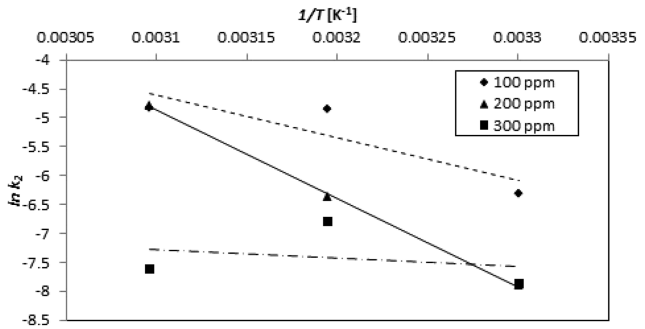

FIG. 11. The activation energy of the process was evaluated by plotting the pseudo-second-order kinetic model vs 1/T.

visual depiction of how two parameters together affect biosorption (Fig. 13).

The quadratic ideal designed for method development has been shown to be useful in anticipating the maximum adsorption limit and understanding the interactions between self-regulating components and their effects on the adsorption cycle. Measurable progress resulted in an ~70.5% rise in adsorption from 475 to 810 mg g^{-1}.

TABLE VI. Restrictions of the AB113-NICUS method's thermodynamics.

Initial concentration (ppm)	Temperature (K)	ΔG° (KJ mol^{-1})	ΔS° (J^{-1} mol^{-1} K)	ΔH° (kJ^{-1} mol)	ln (A)	E_a (kJ^{-1} mol)
100	303	−8.11	993.08	233.95	18.19	508.50
	313	−9.12				
	323	−10.50				
200	303	−6.36	816.48	194.55	42.49	1055.99
	313	−7.32				
	323	−8.32				
300	303	−7.38	1905.52	97.20	2.90	100.29
	313	−7.97				
	323	−8.64				

06 March 2025 15:32:30

© Author(s) 2024

TABLE VII. ANOVA table.

Source	Sum of squares	Degree of freedom	Mean square	F value	P-value
Model	666 983.2	13	51 306.4	112.1	<0.001[a]
A	26 505.2	1	26 505.2	57.9	<0.001[a]
B	2659.0	1	2659.0	5.8	0.018[b]
C	242 410.8	1	242 410.8	529.6	<0.001[a]
D	40 689.5	1	40 689.5	88.9	<0.001[a]
E	24 020.6	1	24 020.6	52.5	<0.001[a]
AB	697.7	1	697.7	1.5	0.2201[c]
AC	20 187.6	1	20 187.6	44.1	<0.001[a]
BC	4821.6	1	4821.6	10.5	<0.001[a]
A^2	26 899.9	1	26 899.9	58.8	<0.0001[c]
B^2	2656.8	1	2656.8	5.8	0.018[b]
C^2	0.02	1	0.02	0.000 04	0.9947[c]
D^2	12 378.1	1	12 378.1	27.0	<0.001[a]
E^2	4943.2	1	4943.2	10.8	<0.001[a]
Residual	41 649.8	91	457.7		
Total	708 633.0	104			

[a]Strongly significa (p value: $p \leq 0.01$).
[b]Moderately significant (p value: $0.01 < p \leq 0.05$).
[c]Suggestive significance (p value: $0.05 < p < 0.10$).

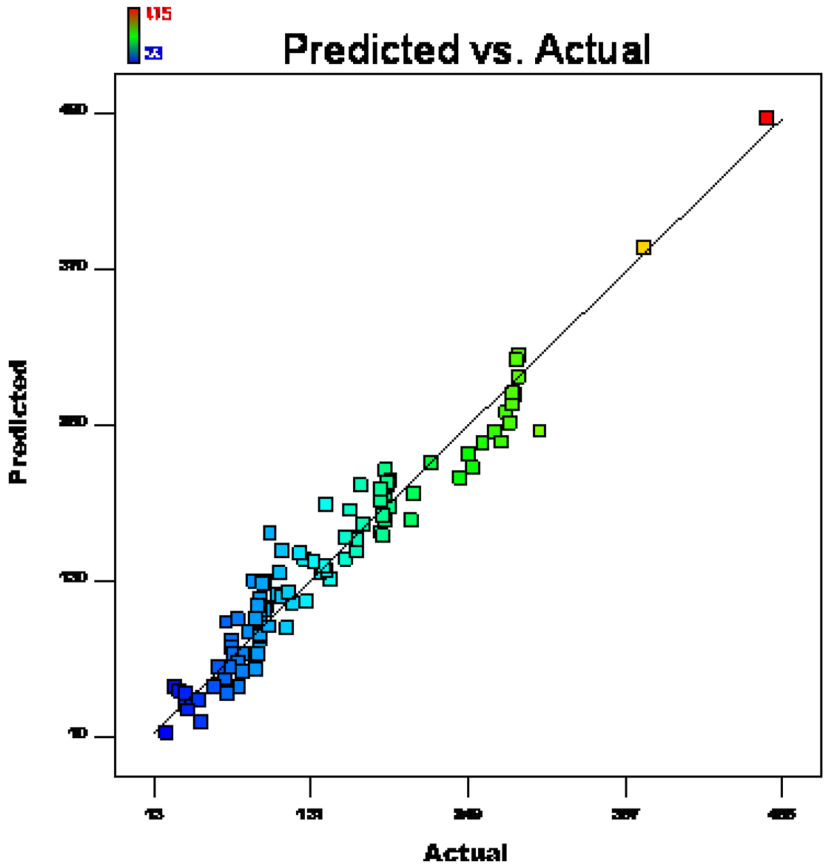

FIG. 12. A chart that contrasts actual and predicted values.

06 March 2025 15:32:30

© Author(s) 2024

a)

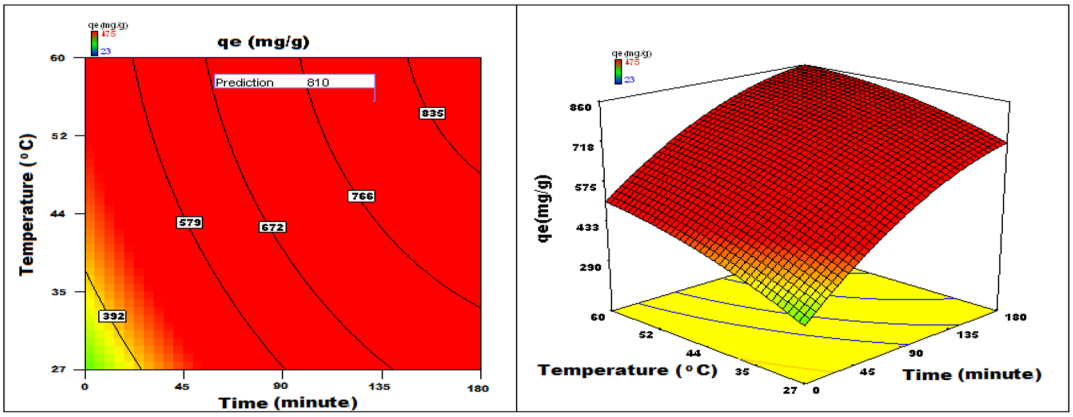

b)

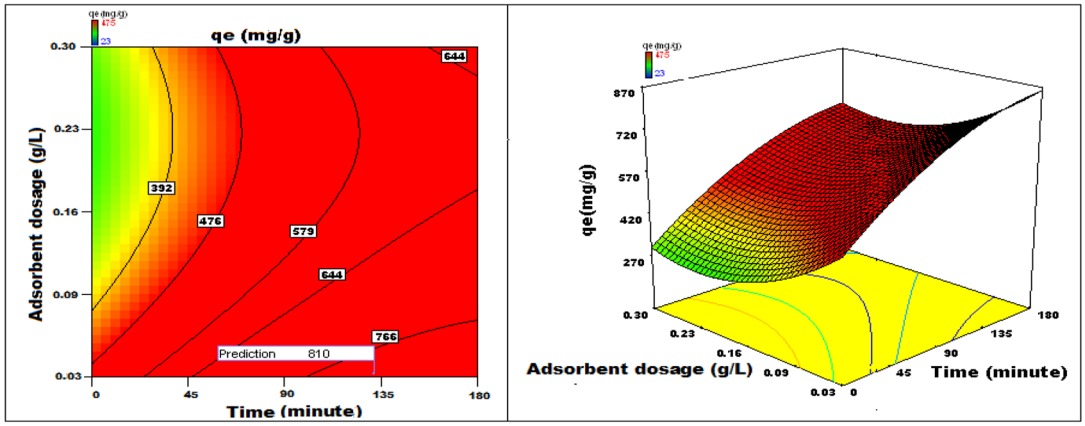

c)

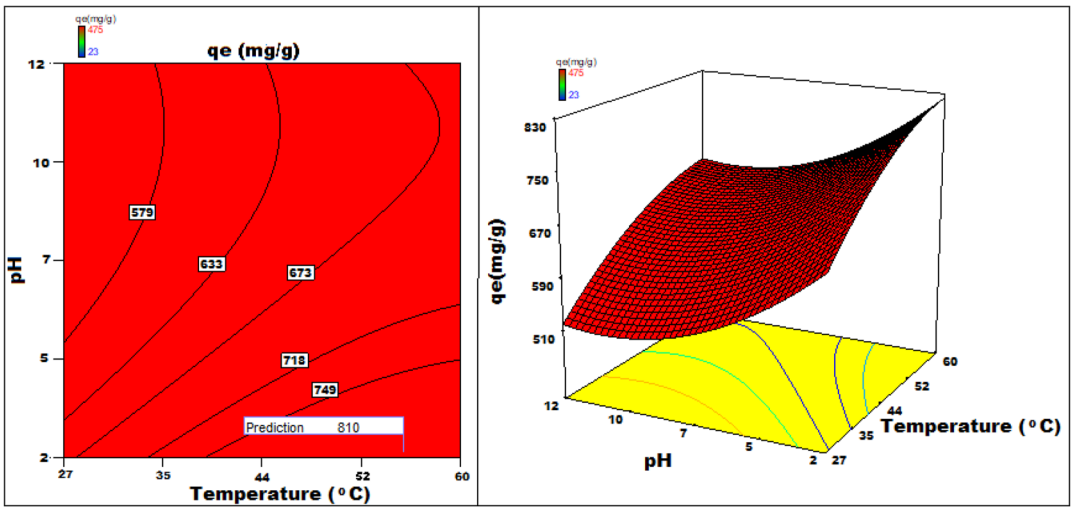

FIG. 13. Adsorption capacity variance: (a) temperature vs time, (b) adsorbent dosage vs time, and (c) pH vs temperature.

06 March 2025 15:32:30

© Author(s) 2024

J. Retrieval of the adsorbent and cost investigation

The adsorbed substance can be recovered by recycling dye-loaded NICUS. This solution might not be cost-effective (less than $1 US for 10 kg of NICUS), since the solvent and technique will cost significantly more than the adsorbent employed in the process. Additionally, it will increase the E-factor, which is harmful considering the massive number of toxins in the environment (Sheldon, 1992).

IV. CONCLUSIONS

At equilibrium conditions, the maximum experimental adsorption capacity (q_e) achieved for NICUS and AB113 dye was determined to be 96 mg g^{-1}. This capacity was investigated using nine different isotherm models to gain a comprehensive understanding of the adsorption process. Based on the findings, the adsorption kinetics followed the pseudo-second-order model, representing that the interactions between NICUS and AB113 dye were primarily physical in nature. This suggests that the adsorption process involved chemisorption or strong van der Waals forces between the dye particles and the adsorbent external. The laboratory testing validated the efficacy of NICUS in treating textile sector effluents, highlighting its potential for practical applications in environmental clean-up. This ongoing study establishes NICUS derived from nutraceutical industrial cumin seed as a promising material for adsorption processes. Moreover, the study underscores the importance of modeling studies in optimizing adsorption processes across various scales, from laboratory experiments to industrial applications. By employing statistical optimization techniques, the research contributes to advancing the efficiency and effectiveness of using NICUS for environmental remediation purposes.

ACKNOWLEDGMENTS

Authors would like to acknowledge the support provided by Researchers Supporting Project Number RSP2024R424 King Saud University, Riyadh Saudi Arabia.

AUTHOR DECLARATIONS

Conflict of Interest

The authors have no conflicts to disclose.

Author Contributions

Syed Noeman Taqui: Conceptualization (equal); Data curation (equal). **Usman Taqui Syed**: Conceptualization (equal); Data curation (equal). **Sameer Algburi**: Conceptualization (equal); Formal analysis (equal). **Rayees Afzal Mir**: Conceptualization (equal); Data curation (equal). **Akheel Ahmed Syed**: Conceptualization (equal); Formal analysis (equal). **Abdullah I. Al-Mansour**: Formal analysis (equal); Investigation (equal). **Shamshad Alam**: Conceptualization (equal); Formal analysis (equal). **Mohammad Amir khan**: Conceptualization (equal); Data curation (equal). **Shareefraza J. Ukkund**: Conceptualization (equal); Data curation (equal); Formal analysis (equal).

DATA AVAILABILITY

The data that support the findings of this study are available from the corresponding authors upon reasonable request.

REFERENCES

[1]O. Merah, B. Sayed-Ahmad, T. Talou, Z. Saad, M. Cerny, S. Grivot, P. Evon, and A. Hijazi, "Biochemical composition of cumin seeds, and biorefining study," Biomolecules **10**(7), 1054 (2020).
[2]K. B. Arun, J. Chandran, V. V. Venugopal, T. S. Madhavankutty, and P. Nisha, "Spent cumin seeds generated from ayurvedic industry as a source of bioactive compounds for nutraceutical/functional food applications," J. Food Proc. Preserv. **42**(1), e13392 (2018).
[3]M. D. Meena, M. K. Vishal, and M. A. Khan, "Market arrivals and prices behaviour of cumin in India," Int. J. Current Microbiol. Appl. Sci. **10**(1), 528–536 (2021).
[4]Z. Chaudhry, R. A. Khera, M. A. Hanif, M. A. Ayub, and S. H. Sumrra, "Cumin," in *Medicinal Plants of South Asia* (Elsevier, 2020), pp. 165–178.
[5]R. P. Singh, H. V. Gangadharappa and K. Mruthunjaya, "Cuminum cyminum – A popular spice: An updated review," Pharmacogn. J. **9**(3), 292 (2017).
[6]S. Pashaei, S. Hosseinzadeh, and A. A. Syed, "Studies on coconut shell powder and crysnanoclay incorporated acrylonitrile-butadiene rubber/styrene butadiene rubber (NBR/SBR) green nanocomposites," Polym. Compos. **38**(4), 727–735 (2017).
[7]S. N. C. S. M. Taqui, M. S. Goodarzi, M. A. Elkotb, B. A. Khatoon, M. E. M. Soudagar, I. B. Koki, A. Elfasakhany, A. S. Khalifa, M. A. Ali, Z. Saifullah, M. I. H. Siddiqui, M. R. Safaei, and C. A. Saleel, "Sustainable adsorption method for the remediation of crystal violet dye using nutraceutical industrial fenugreek seed spent," Appl. Sci. **11**(16), 7635 (2021).
[8]S. N. Taqui, R. Yahya, A. Hassan, N. Nayak, and A. A. Syed, "Adsorption of Acid Blue 113 from aqueous solution onto nutraceutical industrial coriander seed spent: Isotherm, kinetics, thermodynamics and modeling studies," Desalin. Water Treat. **153**, 321–337 (2019).
[9]S. N. Taqui, U. T. Syed, R. T. Syed, M. S. Alqahtani, M. Abbas, and A. A. Syed, "Bioremediation of textile industrial effluents using nutraceutical industrial spent: Laboratory-scale demonstration of circular economy," Nanomaterials **12**(10), 1684 (2022).
[10]M. R. H Mas Har and K. Sathasivam, "The removal of methyl red from aqueous solutions using banana pseudostem fibers," Am. J. Appl. Sci. **6**(9), 1690 (2009).
[11]R. Kumar, M. O. Ansari, and M. A. Barakat, "Adsorption of brilliant green by surfactant doped polyaniline/MWCNTs composite: Evaluation of the kinetic, thermodynamic, and isotherm," Ind. Eng. Chem. Res. **53**(17), 7167–7175 (2014).
[12]M. Suhail, Z. N. Kadhim, and A. H. Al-Mowali, "Bismuth oxyiodide nanocomposites supported on strontium hydroxyapatite enhance UV-Vis light-driven photocatalytic activity," Al-Kitab J. Pure Sci. **6**, 14–29 (2022).
[13]S. Chowdhury and P. Das, "Utilization of a domestic waste—Eggshells for removal of hazardous malachite green from aqueous solutions," Environ. Prog. Sustainable Energy **31**(3), 415–425 (2012).
[14]I. Langmuir, "The constitution and fundamental properties of solids and liquids. Part I. Solids," J. Am. Chem. Soc. **38**(11), 2221–2295 (1916).
[15]R. A. Jawad and R. A. Abd Alwaahed, "Study of the effect of thin layer thickness on the structural properties of copper phthalocyanine (CuPc) films prepared by vacuum thermal Evaporation Method," Al-Kitab J. Pure Sci. **8**(01), 81–91 (2024).
[16]H. M. F. Freundlich, "Over the adsorption in solution," J. Phys. Chem. **57**(385471), 1100–1107 (1906).
[17]D. S. Jovanović, "Physical adsorption of gases," Kolloid Z. Z. Polym. **235**(1), 1203–1213 (1969).
[18]O. J. D. L. Redlich and D. L. Peterson, "A useful adsorption isotherm," J. Phys. Chem. **63**(6), 1024 (1959).
[19]F. Brouers, O. Sotolongo, F. Marquez, and J. P. Pirard, "Microporous and heterogeneous surface adsorption isotherms arising from Levy distributions," Physica A **349**(1-2), 271–282 (2005).
[20]W. R. Vieth and K. J. Sladek, "A model for diffusion in a glassy polymer," J. Colloid Sci. **20**(9), 1014–1033 (1965).

06 March 2025 15:32:30

© Author(s) 2024

[21] R. Sips, "On the structure of a catalyst surface," J. Chem. Phys. **16**(5), 490–495 (1948).
[22] J. Toth, "State equation of the solid-gas interface layers," Acta Chim. Hung. **69**, 311–328 (1971).
[23] C. J. Radke and J. M. Prausnitz, "Thermodynamics of multi-solute adsorption from dilute liquid solutions," AIChE J. **18**(4), 761–768 (1972).
[24] S. K. Lagergren, "About the theory of so-called adsorption of soluble substances," Sven. Vetenskapsakad. Handingarl. **24**, 1–39 (1898).
[25] Y. S. Ho and G. McKay, "Sorption of dye from aqueous solution by peat," Chem. Eng. J. **70**(2), 115–124 (1998).
[26] M. Alkan, Ö. Demirbaş, and M. Doğan, "Adsorption kinetics and thermodynamics of an anionic dye onto sepiolite," Microporous Mesoporous Mater. **101**(3), 388–396 (2007).
[27] H. L. Wang, J. L. Chen, and Z. C. Zhai, "Study on thermodynamics and kinetics of adsorption of p-toluidine from aqueous solution by hypercrosslinked polymeric adsorbents," Environ. Chem. **23**(2), 188–192 (2004).
[28] G. E. Boyd, A. W. Adamson, and L. S. Myers, Jr., "The exchange adsorption of ions from aqueous solutions by organic zeolites. II. Kinetics1," J. Am. Chem. Soc. **69**(11), 2836–2848 (1947).

06 March 2025 15:32:30

© Author(s) 2024